

Relativistic Description of Finite Nuclei Based on Realistic NN Interactions.

E. N. E. van Dalen* and H. Mütter
*Institut für Theoretische Physik, Universität Tübingen,
 Auf der Morgenstelle 14, D-72076 Tübingen, Germany*

A set of relativistic mean field models is constructed including the Hartree and Hartree-Fock approximation accounting for the exchange of isoscalar and isovector mesons as well as the pion. Density dependent coupling functions are determined to reproduce the components of the nucleon self-energy at the Fermi surface, obtained within the Dirac-Brueckner-Hartree-Fock (DBHF) approach using a realistic nucleon-nucleon interaction. It is investigated, to which extend the various mean field models can reproduce the DBHF results for the momentum dependence of the self-energies and the total energy of infinite matter. The mean field models are also used to evaluate the bulk properties of spherical closed-shell nuclei. We find that the Hartree-Fock model allowing for the exchange of σ , ω , ρ , δ mesons and pions, yield the best reproduction of the DBHF results in infinite matter and also provides a good description of the properties of finite nuclei without any adjustment of parameters.

PACS numbers: 21.60.Jz, 21.65.Cd, 21.10.Dr, 21.10.Ft

I. INTRODUCTION

One of the main challenges of theoretical nuclear physics is the attempt to develop a microscopic theory, i.e. without any adjustment of parameters, for the description of bulk properties of finite nuclei, which is based on high precision free space nucleon-nucleon (NN) interactions. This means that this approach connects properties of baryons in the vacuum (NN scattering data) with nuclear systems at densities around the saturation density of nuclear matter. Therefore, this approach should have a high predictive power, when it is used in extreme cases such as in highly isospin asymmetric nuclear systems. The study of these exotic nuclear systems is a fast-growing field of physics. The great scientific potential is demonstrated by the plans for large-scale exotic-nuclear-beam facilities, such as the future GSI facility in Germany, and is driven by the expectation of observing nuclear properties, which are very different from those encountered so far, i.e. near the valley of stability.

However, most of these attempts have already failed in completing the first milestone, which is the microscopic description of the saturation properties of infinite nuclear matter in terms of such free space NN interactions[1–4]. Therefore three-nucleon forces have been introduced to fit the saturation point and/or properties of light nuclei[5, 6]. Relativistic many-body approaches, in particular the Dirac-Brueckner-Hartree-Fock (DBHF) approach, however, have been successful in describing the saturation properties of nuclear matter [7–17] without the necessity to introduce many-body forces. Therefore a significant part of the 3-body terms, which are required in non-relativistic investigations, may represent the relativistic effects originating from the so-called Z-graphs in the expansion of relativistic propagators[18, 19].

Although DBHF calculations have been quite successful in describing nuclear matter, full Dirac Brueckner calculations are still too complex to allow an application to finite nuclei at present, since the consistent treatment of correlation and relativistic effects for finite systems is a rather involved problem. In fact, Van Giai et al. [20] addressed this problem as one of the main open problems in Nuclear Physics. Different approximation schemes have been developed, which treat either the relativistic effects or the correlation effects in an approximative way.

In the former approximation scheme, the Dirac effects are treated via a kind of local density approximation (LDA), whereas the correlations effects are taken into account by solving the Bethe-Goldstone equation directly for the finite nucleus under consideration [17, 21–23]. This means that the self-consistency requirements of a conventional BHF calculation for a finite nucleus are satisfied, while the relativistic effects are taken into account by evaluating the matrix elements of the potential in terms of in-medium Dirac spinors.

In the latter approximation scheme, the Dirac effects are treated directly for the finite nucleus, whereas the correlation effects are deduced from nuclear matter via a local density approximation. This treatment of the correlation effects can be accomplished by defining effective meson exchange interactions, which are obtained from the Dirac-Brueckner self-energy components. Therefore, the coupling constants of such an effective interaction are density dependent, since

*Electronic address: eric.van-dalen@uni-tuebingen.de

these self-energy components are density dependent [24]. In this way, a semi-phenomenological relativistic density functional can be constructed. This approximation scheme to describe finite nuclei will be further explored in this paper.

These semi-phenomenological relativistic density functionals can be divided into two groups, semi-phenomenological density dependent relativistic Hartree (DDRH) theories and semi-phenomenological density dependent relativistic Hartree-Fock (DDRHF) theories. However, between the semi-phenomenological DDRH theories and the DBHF approach two essential differences exist concerning the structure of the self-energy in nuclear matter [15, 17]. The first difference is the absence of a spatial contribution of the vector self-energy Σ_V in the DDRH theory, which is present in the DBHF approach. This self-energy component originates from Fock exchange contributions which are not present in the DDRH theory. The second difference is that the DBHF self-energy terms explicitly depend on the particle's momentum, a feature which is also absent in the DDRH theory. This momentum dependence reflects the non-locality of the DBHF self-energy terms, which originates as well from the Fock exchange terms as from non-localities in the underlying effective NN interaction, the G -matrix. In the work of Ref. [15, 25, 26], renormalizations were introduced to compensate for these differences. However, a more fundamental solution at the level of the structure of the self-energy is preferable and will be investigated in this study.

An improvement of the simple mean field studies of the DDRH studies is the density dependent relativistic Hartree-Fock (DDRHF) theory with its inclusion of the Fock terms, since the essential differences between the DBHF approach and the DDRH theory concerning the structure of the self-energy in nuclear matter discussed above may be cured by the inclusion of the Fock exchange terms. Due to the presence of Fock terms in the DDRHF theory, one obtains a spatial contribution of the vector self-energy Σ_V and momentum dependent self-energy components as in the DBHF approach. However, first attempts of such DDRHF models based on microscopic approaches were not so successful as the DDRH models [27, 28]. A possible reason is that only the isoscalar coupling functions are density dependent and the other coupling functions, such as of the π -meson and the ρ -meson, remain density independent in these DDRHF theories [27, 28]. In addition, the δ -meson is absent in these DDRHF theories. However, in DDRH theories this coupling provides a mechanism to account for the differences in the scalar self-energies, i.e. in the corresponding effective Dirac masses, for neutrons and protons in isospin asymmetric nuclear matter [29]. Therefore, the DDRHF theories can be further improved by including the isovector δ -meson and extend the density dependence to all coupling functions, which has not been done so far for DDRHF theories based on microscopic calculations.

The aim of this study is not to provide an “optimal” DDRHF parameterization, which could then be used in studies of finite nuclei. Instead we are investigating various models, which are all fitted to reproduce the DBHF results for the relativistic components of the nucleon self-energy at the Fermi surface. We then compare these models in predicting other observables for nuclear matter and finite nuclei. Therefore it is the aim to explore the limits and the reliability of such DDRHF description to provide a reliable approximation scheme for a Dirac-Brueckner-Hartree-Fock description of finite nuclei.

The plan of this paper is as follows. The relativistic DDRHF theory is discussed in Sec. II, which also introduces the various stages of the meson exchange models considered and the resulting parameterization of the density-dependent coupling constants. Results for the structure of infinite matter and finite nuclei are presented and discussed in Sec. III. Finally, we end with a summary and the conclusion in Sec. IV.

II. DENSITY DEPENDENT RELATIVISTIC HARTREE-FOCK.

A Lagrangian density of an interacting many-particle system consisting of nucleons and mesons is the starting point of a DDRHF theory. The Lagrangian density of the DDRHF theory presented here includes as well the isoscalar mesons σ and ω as the isovector mesons δ and ρ . Furthermore, one has the pseudo-vector meson π . Therefore, the Lagrangian density consists of three parts: the free baryon Lagrangian density \mathcal{L}_B , the free meson Lagrangian density \mathcal{L}_M , and the interaction Lagrangian density \mathcal{L}_{int} :

$$\mathcal{L} = \mathcal{L}_B + \mathcal{L}_M + \mathcal{L}_{\text{int}}, \quad (1)$$

which takes on the explicit form

$$\mathcal{L}_B = \bar{\Psi}(i\gamma_\mu\partial^\mu - M)\Psi, \quad (2)$$

$$\mathcal{L}_M = \frac{1}{2} \sum_{\iota=\sigma,\delta,\pi} \left(\partial_\mu \Phi_\iota \partial^\mu \Phi_\iota - m_\iota^2 \Phi_\iota^2 \right) - \frac{1}{2} \sum_{\kappa=\omega,\rho} \left(\frac{1}{2} F_{(\kappa)\mu\nu} F_{(\kappa)}^{\mu\nu} - m_\kappa^2 A_{(\kappa)\mu} A_{(\kappa)}^\mu \right), \quad (3)$$

$$\mathcal{L}_{\text{int}} = -g_\sigma \bar{\Psi} \Phi_\sigma \Psi - g_\delta \bar{\Psi} \boldsymbol{\tau} \boldsymbol{\Phi}_\delta \Psi - \frac{f_\pi}{m_\pi} \bar{\Psi} \boldsymbol{\tau} \gamma_5 \boldsymbol{\gamma}_\mu [\partial^\mu \boldsymbol{\Phi}_\pi] \Psi - g_\omega \bar{\Psi} \gamma_\mu A_{(\omega)}^\mu \Psi - g_\rho \bar{\Psi} \boldsymbol{\tau} \gamma_\mu \mathbf{A}_{(\rho)}^\mu \Psi \quad (4)$$

with the field strength tensor $F_{(\kappa)\mu\nu} = \partial_\mu A_{(\kappa)\nu} - \partial_\nu A_{(\kappa)\mu}$ for the vector mesons. In the above Lagrangian density the nucleon field is denoted by Ψ and the nucleon rest mass by M . The scalar meson fields are Φ_σ and Φ_δ and the vector meson fields are $A_{(\omega)}$ and $A_{(\rho)}$. Furthermore, the pseudo-vector π field is denoted by Φ_π . Moreover, the bold symbols denote vectors in the isospin space acting between the two species of nucleons. The mesons have rest masses m_σ , m_ω , m_δ , m_ρ , and m_π and couple to the nucleons with the strength of the coupling constants g_σ , g_δ , g_ω , g_ρ , and f_π .

A. Nuclear Matter

To obtain the field equations for the nucleons, we minimize the action for variations of the fields $\bar{\Psi}$ included in the Lagrangian density of Eq. (1)

$$\delta \int_{t_0}^{t_1} dt \int d^3x \mathcal{L}(\bar{\Psi}(x), \partial_\mu \bar{\Psi}(x), t) = 0. \quad (5)$$

Finally the following field equation is obtained

$$\frac{\partial}{\partial x^\mu} \frac{\partial \mathcal{L}}{\partial (\partial_\mu \bar{\Psi})} - \frac{\partial \mathcal{L}}{\partial \bar{\Psi}} - \frac{\partial \mathcal{L}}{\partial \rho} \frac{\delta \rho}{\delta \bar{\Psi}} = 0. \quad (6)$$

Without density dependent meson-baryon vertices, Eq. (6) reduces to the normal Euler-Lagrange field equation, since the third term vanishes. Evaluating Eq. (6) for the field $\bar{\Psi}$, we obtain the Dirac equation. This Dirac equation for the nucleon field can be written as

$$(i\gamma_\mu \partial^\mu - M - (\Sigma + \Sigma^{(r)}\gamma_0)) \Psi = 0, \quad (7)$$

where Σ is the nucleon self-energy and $\Sigma^{(r)}$ is the so-called rearrangement contribution to the nucleon self-energy.

The self-energy Σ is obtained as well for density dependent as density independent meson-baryon vertices and reads

$$\begin{aligned} \Sigma = & \left(g_\sigma \Phi_\sigma + g_\delta \boldsymbol{\tau} \Phi_\delta + \frac{f_\pi}{m_\pi} \boldsymbol{\tau} \gamma_5 \gamma_\mu [\partial^\mu \Phi_\pi] + g_\omega \gamma_\mu A_{(\omega)}^\mu \right. \\ & \left. + g_\rho \boldsymbol{\tau} \gamma_\mu A_{(\rho)}^\mu \right). \end{aligned} \quad (8)$$

for the Lagrangian density in Eqs. (1)-(4). Furthermore, this nucleon self-energy can be split into different parts with well-defined behavior under Lorentz transformations. Because of the requirement of translational and rotational invariance, hermiticity, parity conservation, and time reversal invariance, the most general form of the Lorentz structure of the self-energy is

$$\Sigma(k) = \Sigma_s(k) - \gamma_0 \Sigma_o(k) + \boldsymbol{\gamma} \cdot \mathbf{k} \Sigma_v(k), \quad (9)$$

where Σ_s , Σ_o , and Σ_v components are Lorentz scalar functions. Therefore, it is practical to define the following effective quantities

$$k^* = k(1 + \Re \Sigma_v(k)), \quad (10)$$

$$m^*(k) = M + \Re \Sigma_s(k), \quad (11)$$

and

$$E^*(k) = E(k) + \Re \Sigma_o(k). \quad (12)$$

In the on-shell case, the effective energy can also be written as

$$E^*(k)^2 = k^{*2} + m^*(k)^2. \quad (13)$$

On the level of the Hartree-Fock approximation, the contributions to the self-energy of the Lagrangian density presented in Eqs. (1)-(4) are

$$\begin{aligned}\Sigma_{s,i}(k) = & -\left(\frac{g_\sigma}{m_\sigma}\right)^2 (\rho_{s,n} + \rho_{s,p}) - \left(\frac{g_\delta}{m_\delta}\right)^2 \sum_{j=n,p} (\rho_{s,i} - \rho_{s,j}) \\ & + \frac{1}{(4\pi)^2} \frac{1}{k} \sum_{j=n,p} \int_0^{k_{Fj}} q dq \frac{m^*(q)}{E^*(q)} \left[\delta_{ij} [g_\sigma^2 \Theta_\sigma(k, q) - 4g_\omega^2 \Theta_\omega(k, q)] \right. \\ & \left. + (2 - \delta_{ij}) \left[-\left(\frac{f_\pi}{m_\pi}\right)^2 m_\pi^2 \Theta_\pi(k, q) - 4g_\rho^2 \Theta_\rho(k, q) + g_\delta^2 \Theta_\delta(k, q) \right] \right],\end{aligned}\quad (14)$$

$$\begin{aligned}\Sigma_{o,i}(k) = & -\left(\frac{g_\omega}{m_\omega}\right)^2 (\rho_n + \rho_p) - \left(\frac{g_\rho}{m_\rho}\right)^2 \sum_{j=n,p} (\rho_i - \rho_j) \\ & - \frac{1}{(4\pi)^2} \frac{1}{k} \sum_{j=n,p} \int_0^{k_{Fj}} q dq \left[\delta_{ij} [g_\sigma^2 \Theta_\sigma(k, q) + 2g_\omega^2 \Theta_\omega(k, q)] \right. \\ & \left. + (2 - \delta_{ij}) \left[-\left(\frac{f_\pi}{m_\pi}\right)^2 m_\pi^2 \Theta_\pi(k, q) + 2g_\rho^2 \Theta_\rho(k, q) + g_\delta^2 \Theta_\delta(k, q) \right] \right],\end{aligned}\quad (15)$$

and

$$\begin{aligned}\Sigma_{v,i}(k) = & -\frac{1}{(4\pi k)^2} \sum_{j=n,p} \int_0^{k_{Fj}} dq \frac{q^*}{E^*(q)} \left[\delta_{ij} [2g_\sigma^2 \Gamma_\sigma(k, q) + 4g_\omega^2 \Gamma_\omega(k, q)] \right. \\ & + (2 - \delta_{ij}) \left[-2 \left(\frac{f_\pi}{m_\pi}\right)^2 ((k^2 + q^2) \Gamma_\pi(k, q) - kq^2 \Theta_\pi(k, q)) + 4g_\rho^2 \Gamma_\rho(k, q) \right. \\ & \left. \left. + 2g_\delta^2 \Gamma_\delta(k, q) \right] \right].\end{aligned}\quad (16)$$

The first two terms in $\Sigma_{s,i}$ and $\Sigma_{o,i}$ correspond to the Hartree contribution with

$$\rho_{s,i} = \frac{1}{\pi^2} \int_0^{k_{Fi}} q^2 dq \frac{m^*(q)}{E^*(q)}, \quad (17)$$

$$\rho_i = \frac{k_{Fi}^3}{3\pi^2} \quad (18)$$

The remaining expressions are due to the Fock contributions, where the abbreviations

$$A(k, q) = q^2 + k^2 - (E(k) - E(q))^2, \quad (19)$$

$$\Theta_i(k, q) = \ln \left(\frac{A(k, q) + m_i^2 + 2kq}{A(k, q) + m_i^2 - 2kq} \right), \quad (20)$$

and

$$\Gamma_i(k, q) = \frac{((A(k, q) + m_i^2) \Theta_i(k, q))}{4k} - q \quad (21)$$

are used.

The $\Sigma^{(r)}$ term in Eq. (7) will only be present, if meson-baryon vertices are density dependent, and is generated by the third term in Eq. (6). This rearrangement contribution $\Sigma^{(r)}$ reads

$$\begin{aligned}\Sigma^{(r)} = & \left(\frac{\partial g_\sigma}{\partial \rho} \bar{\Psi} \Phi_\sigma \Psi + \frac{\partial g_\delta}{\partial \rho} \bar{\Psi} \boldsymbol{\tau} \Phi_\delta \Psi + \frac{1}{m_\pi} \frac{f_\pi}{\partial \rho} \bar{\Psi} \boldsymbol{\tau} \gamma_5 \gamma_\mu [\partial^\mu \Phi_\pi] \Psi \right. \\ & \left. + \frac{\partial g_\omega}{\partial \rho} \bar{\Psi} \gamma_\mu A_{(\omega)}^\mu \Psi + \frac{\partial g_\rho}{\partial \rho} \bar{\Psi} \boldsymbol{\tau} \gamma_\mu \mathbf{A}_{(\rho)}^\mu \Psi \right).\end{aligned}\quad (22)$$

meson i	m [MeV]	a_i	b_i	c_i	d_i
σ	550	9.28996	-0.8403	0.25791	-0.015436
ω	782.6	10.23446	0.23622	-0.1503	0.0297512
σ	550	8.86711	-1.1508	0.39224	-0.034995
ω	782.6	8.37380	0.71233	-0.2986	0.0469882

TABLE I: Parameter set for the $\sigma\omega$ model from the DBHF approach in Ref. [15]. The upper part of the table contains the parameters to be used in the Hartree approach, whereas the lower part refers to the DDRHF model.

meson i	m [MeV]	a_i	b_i	c_i	d_i
σ	550	8.65683	-1.0265	0.35362	-0.0408585
ω	782.6	8.62502	0.53724	-0.2312	0.0386465
π	139	1.00265	-	-	-

TABLE II: Parameter set for the $\sigma\omega\pi$ DDRHF model from the DBHF approach in Ref. [15].

These rearrangement contributions are essential to provide a symmetry conserving approach, which implies that energy-momentum conservation and thermodynamic consistency like the Hugenholtz - van Hove theorem are satisfied[30]. However, these rearrangement terms do not contribute to the energy per nucleon,

$$E/A = T + V - M, \quad (23)$$

where the kinetic energy per nucleon is

$$T = \left[M\rho_s + \frac{1}{\pi^2} \sum_{i=n,p} \int_0^{k_{Fi}} \frac{q^*}{E^*(q)} q^3 dq \right] \frac{1}{\rho_B} \quad (24)$$

and the potential energy per nucleon is

$$V = \frac{1}{2\pi^2\rho_B} \sum_{i=n,p} \int_0^{k_{Fi}} \left(\frac{m^*(q)}{E^*(q)} \Sigma_{s,i}(q) - \Sigma_{o,i}(q) + \frac{q^*}{E^*(q)} q \Sigma_{v,i}(q) \right) q^2 dq, \quad (25)$$

with $\rho_s = \rho_{s,n} + \rho_{s,p}$ and $\rho_B = \rho_n + \rho_p$.

Furthermore, the rearrangement terms can be added to the time-like vector self-energy in Eq. (15). Therefore, it should be noted that these rearrangement terms are sometimes included in the definition of the time-like vector self-energy $\Sigma_0(k)$.

B. Parameterization

We have constructed three different DDRHF models: a $\sigma\omega$ model, a $\sigma\omega\pi$ model, and a $\sigma\omega\pi\rho\delta$ model. The effective coupling constants for the mesons are determined by requesting that the HF expression for the scalar self-energy $\Sigma_s(k)$ and the time-like vector self-energy $\Sigma_0(k)$, i.e. without the rearrangement terms $\Sigma^{(r)}$, calculated at the Fermi surface reproduce the corresponding results of a DBHF calculation using Bonn A [15]. The reason that the rearrangement terms are not included in the fit is that the DBHF approach has no rearrangement contributions. The DBHF data at densities of $\rho_B = 0.100, 0.197, 0.313$, and 0.467 fm^{-3} are used to obtain the parameters of the various models. The density dependent couplings of the $\sigma\omega$ and the $\sigma\omega\pi$ model are obtained from the DBHF results in isospin symmetric nuclear matter ($Y_p = 0.5$), whereas couplings of the $\sigma\omega\pi\rho\delta$ model are determined from results in isospin asymmetric nuclear matter with a proton fraction of $Y_p = 0.4$. For completeness two different Hartree (DDRH) models have been constructed in a similar way.

In order to make these parameterizations easily accessible, we have parameterized the density dependence of the coupling constants by

$$g_i(\rho_B) = a_i + b_i x + c_i x^2 + d_i x^3, \quad (26)$$

meson i	m [MeV]	a_i	b_i	c_i	d_i
σ	550	9.26408	-0.79477	0.24135	-0.013504
ω	782.6	10.18505	0.31476	-0.19474	0.037339
δ	983	9.58644	-4.34658	1.56009	-0.208196
ρ	769	9.51803	-3.36524	1.36753	0.158856
σ	550	4.99231	3.27705	-1.4929	0.230977
ω	782.6	0.67868	10.3068	-4.6471	0.701354
π	139	1.00265	-	-	-
δ	983	12.3664	-8.9781	3.25210	-0.426997
ρ	769	15.2464	-11.1504	4.27083	-0.543179

TABLE III: Parameter set for the $\sigma\omega\pi\rho\delta$ model from the DBHF approach in Ref. [15]. The upper part of the table contains the parameters to be used in the Hartree approach, whereas the lower part refers to the DDRHF model. Note that the π does not contribute in the Hartree approximation.

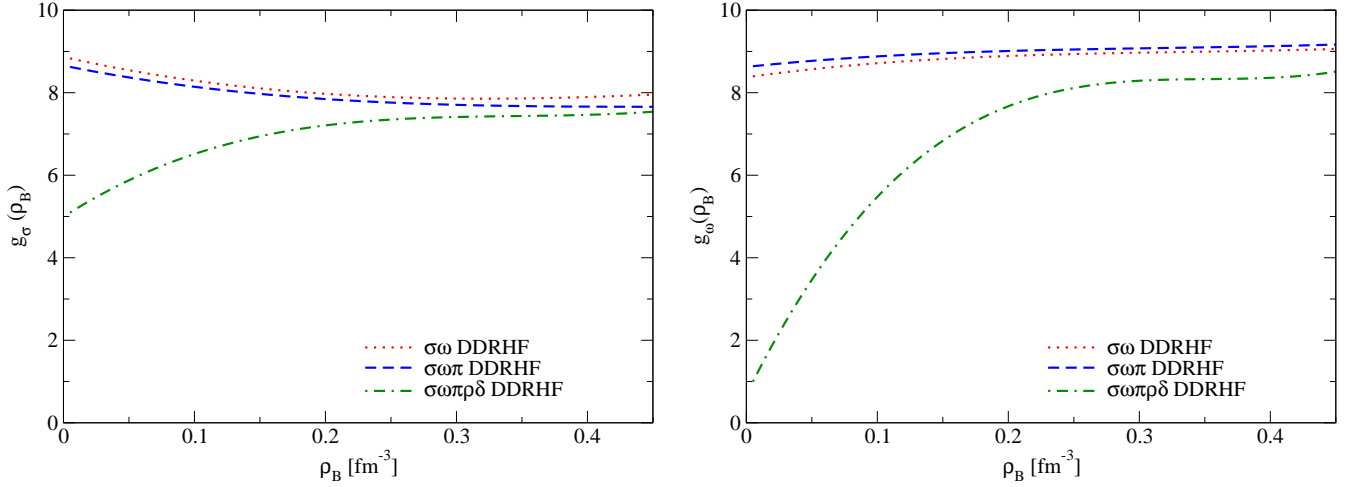


FIG. 1: (Color online) Density dependence of the isoscalar coupling functions of the $\sigma\omega$ (dotted), $\sigma\omega\pi$ (dashed), and the $\sigma\omega\pi\rho\delta$ (dashed-dotted) DDRHF model. Left: the σ coupling function. Right: the ω coupling function.

with $x = \rho_B/\rho_0$ and $\rho_0 = 0.16 \text{ fm}^{-3}$. The parameters of the coupling functions are fitted, except the one of the π coupling function. The π coupling constant is fixed to the free value. In addition, the masses of the mesons are chosen to be identical to those of the Bonn A potential. All parameters are summarized in table I for the $\sigma\omega$ model, in table II for the $\sigma\omega\pi$ model, and in table III for the $\sigma\omega\pi\rho\delta$ model.

The density dependence of the isoscalar coupling functions is displayed in Fig. 1. In the $\sigma\omega$ model, the σ coupling function is decreasing with increasing density, whereas the ω coupling function is slightly increasing with increasing density. These features can be interpreted in the following way:

A significant part of the medium-range attraction contained in the Brueckner G -matrix is due to the iterated π -exchange term. Pauli blocking and dispersive corrections of the nucleon-nucleon propagator in the nuclear medium yield a quenching of these iterated π -exchange terms with increasing density (see e.g. [1] and [2]). In the $\sigma\omega$ model this medium range attraction is described in terms of the σ -exchange. Therefore, the quenching of the iterated π -exchange terms leads to a reduction of the coupling constant for the σ with increasing density.

The same Pauli blocking effects and dispersive corrections in the NN propagator also reduce the correlation effects in the relative wave functions of two nucleons at short distances. Therefore, these short-range correlations are less efficient at higher densities to minimize the repulsive short-range components of the bare NN interaction. This leads to a slight increase of the effective coupling constant for the ω with increasing density.

Next, we will compare the isoscalar coupling functions of the $\sigma\omega$ model with that of the $\sigma\omega\pi$ model. One finds that the inclusion of the π exchange has a small effect on the isoscalar coupling functions, i.e. the σ coupling function is slightly decreased, whereas the ω coupling function is slightly enhanced compared to the $\sigma\omega$ model.

However, in the $\sigma\omega\pi\rho\delta$ model the density dependence of the isoscalar coupling functions dramatically change

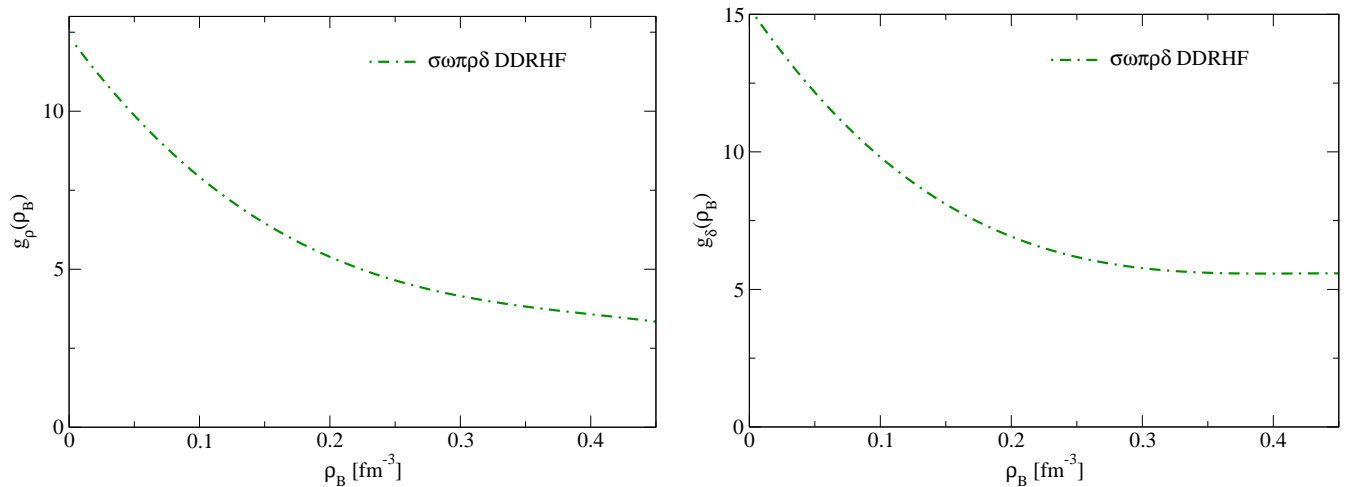


FIG. 2: (Color online) Density dependence of the isovector coupling functions of the $\sigma\omega\pi\rho\delta$ DDRHF model. Left: the ρ coupling function. Right: the δ coupling function.

compared to the $\sigma\omega$ model and the $\sigma\omega\pi$ model. The effective coupling constants for the isovector mesons are rather large in particular at small densities as displayed in Fig. 2. This reflects the significant differences between the isospin $T = 1$ and $T = 0$ interaction, which is required to describe nucleon self-energies in isospin asymmetric nuclear matter. The resulting interplay between the exchange terms for isoscalar and isovector mesons spoils the simple picture to explain the density dependence of the coupling constants for the scalar mesons discussed above.

III. RESULTS AND DISCUSSION

A. Nuclear Matter

In this section we will present the nuclear matter results of the previously constructed DDRHF models and compare them to the original DBHF approach of Ref. [15], which the various parameterizations attempt to reproduce. First, the momentum dependence of the DDRHF self-energy components will be considered. Note that the parameterizations are fitted to the self-energy components at the Fermi momentum k_F . The momentum dependence of the DDRHF self-energies exclusively originates from the various Fock exchange terms, whereas the momentum dependence of the original DBHF self-energies is due to Fock exchange terms but also due to the non-locality and energy-dependence of the underlying G -matrix.

This momentum dependence of the self-energy components in isospin symmetric nuclear matter of a density $\rho_B = 0.197 \text{ fm}^{-3}$ for the various DDRHF models is displayed in Fig. 3. The Hartree approximation ignores all Fock exchange terms and therefore provides a scalar self-energy which is independent on the nucleon momentum k . Also for the $\sigma\omega$ DDRHF model, the scalar self-energy Σ_s turns out to be almost momentum independent. The inclusion of the π improves the momentum dependence of the scalar self-energy Σ_s .

However, for the time-like vector self-energy Σ_0 the opposite behavior can be observed, i.e. the inclusion of the π deteriorates the results. Therefore, a $\sigma\omega\pi$ DDRHF model will in principle not be able to reproduce the momentum dependence of the DBHF self-energy components. Although the momentum dependence in the $\sigma\omega\pi\rho\delta$ model is in better agreement with the DBHF approach than in the other two models, its momentum dependence is only about one half of the momentum dependence observed in the DBHF approach.

As the models are fitted to reproduce the values of the the self-energy components at the Fermi momentum $k = k_F = 1.43 \text{ fm}^{-3}$ all models converge at this point. The $\sigma\omega\pi\rho\delta$ DDRHF model is fitted in isospin asymmetric nuclear matter, therefore a small deviation for this DDRHF model can be observed in isospin symmetric nuclear matter.

The other essential difference between the relativistic Hartree model DDRH and the DBHF approach is the absence of a spatial contribution of the vector self-energy Σ_V in the DDRH theory. Such a contribution is present in the DDRHF theory due to the Fock exchange terms. In our procedure to determine the various DDRHF models this self-energy component is not fitted. Results of various parameterizations are displayed in Fig. 4. One observes that

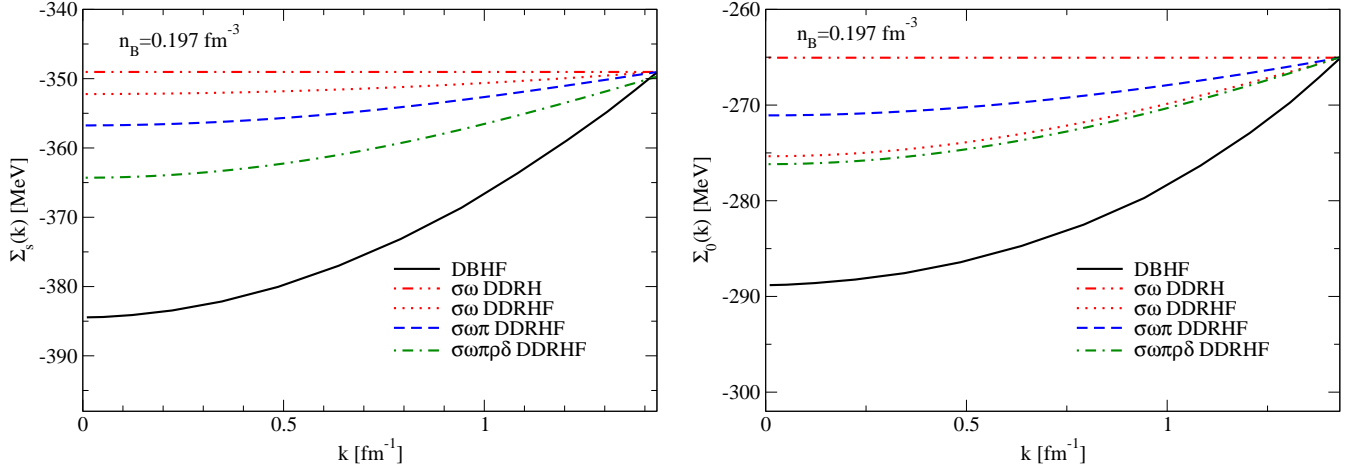


FIG. 3: (Color online) Momentum dependence of the scalar self-energy Σ_s and the time-like vector self-energy Σ_0 for the $\sigma\omega$ (dotted), $\sigma\omega\pi$ (dashed), and the $\sigma\omega\pi\rho\delta$ (dashed-dotted) DDRHF model is plotted at a density of $\rho_B = 0.197 \text{ fm}^{-3}$. In addition, the Hartree model with σ and ω mesons (dashed-dotted dotted) is given. Furthermore, the corresponding self-energy components of the DBHF approach in Ref. [15] (solid line) are presented in this figure. Left: the scalar self-energy Σ_s . Right: the time-like vector self-energy Σ_0 .

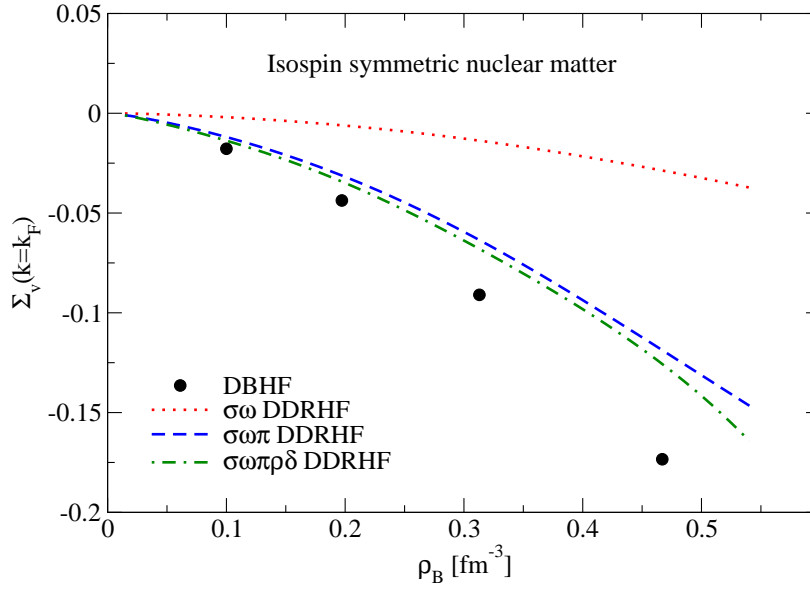


FIG. 4: (Color online) Density dependence of the spatial vector self-energy Σ_v for the $\sigma\omega$ (dotted), $\sigma\omega\pi$ (dashed), and the $\sigma\omega\pi\rho\delta$ (dashed-dotted) DDRHF model is plotted in isospin symmetric nuclear matter. In addition, the corresponding self-energy component of the DBHF approach in Ref. [15] is presented in this figure.

the models with π exchange yield a stronger spatial component and show a much better agreement with the DBHF result than the $\sigma\omega$ model. Therefore, it can be concluded that the inclusion of the π exchange in DDRHF models is essential in reproducing the spatial vector self-energy.

The self-energy components are needed to calculate the energy per nucleon as can be seen from the Eqs. (23)-(25). The energy per nucleon for isospin symmetric nuclear matter and pure neutron matter are displayed in Fig. 5. The various approximation schemes reproduce the DBHF results for symmetric matter reasonably well at medium and larger densities. At densities below 0.8 fm^{-3} all parameterizations tend to underestimate the binding energy per nucleon calculated in the DBHF approach. The $\sigma\omega$ model is less attractive than the DBHF and the other approaches at larger densities. This is partly due to the weak spatial vector component but also due to the fact that the difference between the self-energy components Σ_s and Σ_0 tends to be too small at low momenta in this approach as can be seen

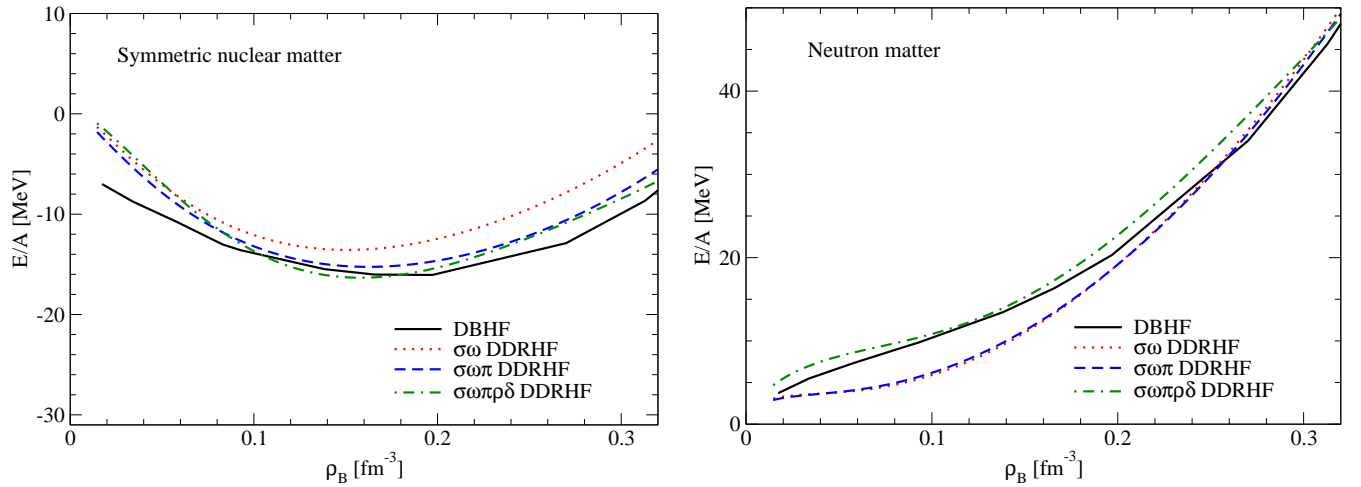


FIG. 5: (Color online) Energy per Nucleon is plotted as a function of the density for the $\sigma\omega$ (dotted), $\sigma\omega\pi$ (dashed), and the $\sigma\omega\pi\rho\delta$ (dashed-dotted) DDRHF model. In addition, the energy per nucleon of the DBHF approach in Ref. [15] (solid line) is given. Left: isospin symmetric nuclear matter. Right: pure neutron matter.

	Hartree		DDRHF			DBHF
	$\sigma\omega$	$\sigma\omega\pi\rho\delta$	$\sigma\omega$	$\sigma\omega\pi$	$\sigma\omega\pi\rho\delta$	
ρ_0 [fm $^{-3}$]	0.1572	0.1613	0.1508	0.1623	0.1583	0.181
E/A [MeV]	-14.44	-14.76	-13.56	-15.25	-16.34	-16.15

TABLE IV: Saturation properties of nuclear matter for the various models compared to the DBHF results of Ref. [14, 15]. The quantities listed include the saturation density ρ_0 and the binding energy E/A at saturation density.

in Fig. 3.

Therefore, at saturation density nuclear matter is too weakly bound as can be seen in Table. IV. In addition, the saturation density is shifted to lower densities compared to the original DBHF results. This shift of the saturation density to a lower density than in the DBHF approach is also observed in the other DDRHF models.

For pure neutron matter, one finds in Fig. 5 that the isovector mesons ρ and δ are important to describe the DBHF results at low densities in particular. The influence of these mesons gets smaller at high densities, which is already indicated by the density-dependence of the coupling constants shown in Fig. 2.

B. Finite Nuclei

For the study of finite nuclei, we account for the density dependent correlation effects in a relativistic HF calculation by employing the coupling constants calculated at the local density. The density profile $\rho_B(r)$ is determined from the result of the relativistic HF calculation in a self-consistent manner [27]. Furthermore, the rearrangement self-energy contribution is taken into account, since it is important to get appropriate single-particle energies and wave functions in finite nuclei. To solve the Dirac equation for finite nuclei in coordinate space, the radial functions are expanded in a discrete basis of spherical Bessel functions. This discrete basis forms a complete orthonormal basis in a sphere of radius D . This radius D is chosen to be 30 fm, which is large enough to ensure that the results for the bound single-particle states are independent on D .

We have investigated some closed-shell nuclei with our DDRHF model. The results obtained for the binding energy and charge radius are presented in Table V. The center of mass correction is included in the displayed binding energies and the charge radii have been evaluated from the proton density, assuming a radius of 0.8 fm for the charge radius of the proton.

The $\sigma\omega$ DDRHF model yields with too little binding for all nuclei considered. This outcome is expected from the nuclear matter results, since this model is too repulsive in symmetric nuclear matter as can be seen in Fig. 5. The explicit inclusion of the π -exchange improves the results substantially. The $\sigma\omega\pi\rho\delta$ model yields too much binding

Nucleus	Hartree		Hartree		DDRHF		DDRHF		DDRHF		Exp.	
	$\sigma\omega$		$\sigma\omega\pi\rho\delta$		$\sigma\omega$		$\sigma\omega\pi$		$\sigma\omega\pi\rho\delta$			
	E/A	r_{CD}	E/A	r_{CD}	E/A	r_{CD}	E/A	r_{CD}	E/A	r_{CD}	E/A	r_{CD}
^{16}O	-6.49	2.75	-6.65	2.72	-6.00	2.77	-7.63	2.67	-8.91	2.62	-7.98	2.74
^{40}Ca	-7.10	3.47	-7.29	3.43	-6.54	3.49	-8.08	3.39	-9.18	3.34	-8.55	3.48
^{48}Ca	-7.29	3.51	-7.20	3.47	-6.64	3.53	-7.67	3.43	-8.81	3.40	-8.67	3.47
^{90}Zr	-7.20	4.29	-7.26	4.23	-6.56	4.32	-7.70	4.20	-8.83	4.16	-8.71	4.27

TABLE V: Results for the binding energies per nucleon in MeV and the charge radii in fm for the various DDRH and DDRHF models. The calculated energies have been corrected by subtracting the spurious energy of the center of mass motion. The experimental values are taken from Ref. [25].

Orbital	$\sigma\omega$		$\sigma\omega\pi$		$\sigma\omega\pi\rho\delta$		exp.	
	Proton	Neutron	Proton	Neutron	Proton	Neutron	Proton	Neutron
^{16}O								
$0s_{1/2}$	-27.62	-31.86	-34.64	-39.05	-37.06	-41.50	-44±7	-47
$0p_{3/2}$	-13.16	-17.09	-16.55	-20.65	-18.73	-22.90	-18.451	-21.839
$0p_{1/2}$	-9.35	-13.20	-12.75	-16.78	-14.23	-18.34	-12.127	-15.663
^{40}Ca								
$0s_{1/2}$	-33.13	-41.45	-41.28	-49.91	-43.15	-51.77	-49.1±12	
$0p_{3/2}$	-22.11	-30.06	-27.79	-36.00	-30.19	-38.43	-33.3±6.5	
$0p_{1/2}$	-19.55	-27.45	-25.30	-33.47	-27.42	-35.61	-32±4	
$0d_{5/2}$	-10.71	-18.29	-13.62	-21.45	-15.72	-23.64	-14.2±2.5	-21.30
$1s_{1/2}$	-6.70	-14.23	-8.95	-16.78	-9.31	-17.33	-10.850	-18.10
$0d_{3/2}$	-6.61	-14.08	-9.50	-17.23	-11.01	-18.85	-8.325	-15.641
^{48}Ca								
$0s_{1/2}$	-37.17	-42.35	-44.52	-50.90	-48.38	-52.64		
$0p_{3/2}$	-27.25	-31.13	-32.05	-36.84	-36.75	-39.03		
$0p_{1/2}$	-25.18	-29.51	-29.80	-36.46	-34.10	-38.50		
$0d_{5/2}$	-16.32	-19.48	-18.38	-22.09	-23.22	-24.10	-20±1	
$1s_{1/2}$	-11.26	-15.57	-13.03	-18.45	-15.84	-19.08	-15.8	
$0d_{3/2}$	-12.55	-16.18	-14.47	-20.93	-18.68	-22.44	-15.3	
$0f_{7/2}$	(-4.90)	-7.89	(-4.55)	-7.82	(-8.75)	-8.95		

TABLE VI: Single particle energies for the orbital levels of ^{16}O , ^{40}Ca , and ^{48}Ca nucleus derived from RHF calculations using various models. The experimental values are taken from Ref. [27, 31].

energy for the light nuclei, whereas a good agreement to the empirical values is obtained for the heavier nuclei. Furthermore, all models predict charge radii, which are in good agreement with experimental values.

Single particle energies for the orbital levels of the ^{16}O , ^{40}Ca , and ^{48}Ca nucleus are presented in Table VI for the various models. The $\sigma\omega$ DDRHF model predicts absolute values of single-particle energy, which are too small. The single particle energies of the $\sigma\omega\pi$ and $\sigma\omega\pi\rho\delta$ model are in good agreement with experimental data. They are in better agreement with experimental values than the energy levels calculated in Refs. [27, 28], which lie too deep. However, the order of the 1s-shell and 0d-shell deviates from experiment. The spin-orbit splitting plays a key role in the ordering of these shells. The spin-orbit splittings of some nuclei are given in Table VII. It can be seen that in all the presented DDRHF models the spin-orbit splittings in ^{16}O and ^{40}Ca are smaller than the experimental values. However, the agreement is better in ^{48}Ca and in ^{90}Zr , in particular for the $\sigma\omega\pi\rho\delta$ model. In works of Ref. [27, 28], it was reported that the π exchange reduced the spin-orbit splitting. We find as can be seen in Table VII that the inclusion of the π has no noticeable effect on the spin-orbit splitting in light symmetric nuclei, whereas in heavier asymmetric nuclei a small increase in the spin-orbit splitting can be observed. However, the inclusion of the isovector ρ and δ meson leads to a clear increase of the spin-orbit splitting in as well light as heavier nuclei.

Fig. 6 shows the proton density distribution of the ^{16}O nucleus. It is found that in the $\sigma\omega$ model the proton density in the interior is smaller than in the other two models and has a longer tail. Therefore, it has a larger charge radius as can be seen in Table V. Furthermore, the smaller maximum density in the $\sigma\omega$ model compared to the other models

Nucleus	$\sigma\omega$	$\sigma\omega\pi$	$\sigma\omega\pi\rho\delta$	exp.
^{16}O	3.81	3.8	4.5	6.3
^{40}Ca	4.1	4.12	4.71	7.2
^{48}Ca	3.77	3.91	4.54	4.3
^{90}Zr	1.03	1.22	1.51	1.5

TABLE VII: Spin-orbit splittings of protons for the 0p-shell in ^{16}O , the 0d-shell in ^{40}Ca and ^{48}Ca , and the 1p-shell in ^{90}Zr . The experimental values are taken from Ref. [28].

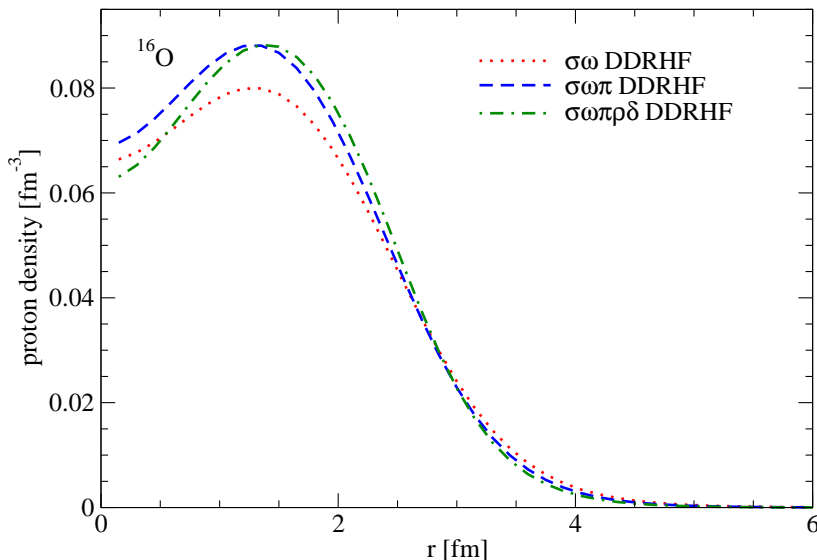


FIG. 6: (Color online) Proton density distribution of ^{16}O nucleus for the $\sigma\omega$ (dotted), $\sigma\omega\pi$ (dashed), and the $\sigma\omega\pi\rho\delta$ (dashed-dotted) DDRHF model.

can be expected from its smaller saturation density in nuclear matter.

IV. SUMMARY AND CONCLUSION

Although Dirac-Brueckner-Hartree-Fock (DBHF) calculations have been quite successful in describing nuclear matter, corresponding DBHF calculations have not yet been performed for finite nuclei as such calculations still seem to be too complex. Various attempts have already been made to approximate such DBHF calculations by employing some kind of local density approximation by parameterizing the results of DBHF calculations of nuclear matter in terms of either a Dirac Hartree (DDRH) model or a Dirac Hartree Fock (DDRHF) model with density-dependent coupling constants for various mesons considered.

It has been the aim of this investigation to compare these different models. The parameters of these DDRH and DDRHF models were all fixed to reproduce at each density the same scalar Σ_s and time-like vector component Σ_0 component of the self-energy obtained in the DBHF calculation for nucleons with momentum equal to the Fermi momentum k_F .

While the DDRH approach yields no momentum dependence of the self-energies, the DDRHF model reproduces the qualitative features of the momentum dependence obtained in the DBHF calculations. However, only 50 percent of this momentum dependence can be related to the Fock exchange terms. The remaining part of the momentum dependence in DBHF is due to the non-locality of the DBHF G -matrix. It remains as a challenge for further investigations to account for this non-locality in such a way that the complete energy- and momentum-dependence of the self-energy is described in nuclear matter using a representation, which can be transferred to calculations of finite nuclei.

The spatial vector component of the nucleon self-energy Σ_v of the DBHF is dominated by the π -exchange term and therefore can be accounted for in DDRHF models, which include the π explicitly. The exchange of isovector mesons ρ and δ is important to describe the differences of correlation effects in isospin $T = 0$ and $T = 1$ channels. Therefore

a DDRHF model accounting for $\sigma, \omega, \pi, \rho$ and δ exchange is required to reproduce the features of DBHF calculations for symmetric and asymmetric nuclear matter.

Fair agreement with empirical data is obtained when this parameterization of the full $\sigma\omega\pi\rho\delta$ model is employed in Dirac Hartree Fock calculations of finite nuclei with density dependent coupling constants for light and heavy nuclei. The parameterization of the coupling constants is presented in form which makes it accessible for other users.

Acknowledgments

This work has been supported by the Deutsche Forschungsgemeinschaft (DFG) under contract no. Mu 705/5-2.

-
- [1] R. Machleidt, *Adv. in Nucl. Phys.* **19**, 189 (1989).
 - [2] H. Mütter and A. Polls, *Prog. Part. and Nucl. Phys.* **45**, 243 (2000).
 - [3] M. Baldo, in *Nuclear Methods and the Nuclear Equation of State*, Vol. 8, p.1 (World Scientific, 1999).
 - [4] F. Coester, S. Cohen, B.D. Day and C.M. Vincent, *Phys. Rev. C* **1**, 769 (1970).
 - [5] W. Zuo, A. Lejeune, U. Lombardo, and J.-F. Mathiot, *Nucl. Phys. A* **706**, 418 (2002).
 - [6] S.K. Bogner, A. Schwenk, R.J. Furnstahl, and A. Nogga, *Nucl. Phys. A* **763**, 59 (2005).
 - [7] M.R. Anastasio, L.S. Celenza, W.S. Pong, and C.M. Shakin, *Phys. Rep.* **100**, 327 (1983).
 - [8] C.J. Horowitz and B.D. Serot, *Nucl. Phys. A* **464**, 613 (1987).
 - [9] B. ter Haar and R. Malfliet, *Phys. Rep.* **149**, 207 (1987).
 - [10] R. Brockmann, R. Machleidt, *Phys. Rev. C* **42**, 1965 (1990).
 - [11] F. de Jong and H. Lenske, *Phys. Rev. C* **58**, 890 (1998).
 - [12] T. Gross-Boelting, C. Fuchs, and Amand Faessler, *Nucl. Phys.* **A648**, 105 (1999).
 - [13] D. Alonso and F. Sammarruca, *Phys. Rev. C* **67**, 054301 (2003).
 - [14] E.N.E. van Dalen, C. Fuchs, and A. Faessler, *Nucl. Phys.* **A744**, 227 (2004).
 - [15] E.N.E. van Dalen, C. Fuchs, and A. Faessler, *Eur.Phys.J. A* **31**, 29 (2007).
 - [16] E.N.E. van Dalen and H. Mütter, *Phys. Rev. C* **82**, 014319 (2010).
 - [17] E.N.E. van Dalen and H. Mütter, *Int. J. Mod. Phys. E* **19**, 2077 (2010).
 - [18] G.E. Brown, W. Weise, G. Baym, and J. Speth, *Comments Nucl. Part. Phys.* **17**, 39 (1987).
 - [19] A. Bouyssy, J.-F. Mathiot, N. van Giai, and S. Marcos, *Phys. Rev. C* **36**, 380 (1987).
 - [20] N. van Giai, B.V. Carlson, Z. Ma, and H.H. Wolter, *J.Phys. G* **37**, 064043 (2010).
 - [21] H. Mütter, R. Machleidt, and R. Brockmann, *Phys. Lett. B* **202**, 483 (1988).
 - [22] H. Mütter, R. Machleidt, and R. Brockmann, *Phys. Rev. C* **42**, 1981 (1990).
 - [23] R. Fritz, H. Mütter, and R. Machleidt, *Phys. Rev. Lett.* **71**, 46 (1993).
 - [24] S. Marcos, R. Niembro, M. López-Quelle, N. Van Giai, and R. Malfliet, *Phys. Rev. C* **39**, 1134 (1989).
 - [25] F. Hoffmann, C.M. Keil, and H. Lenske, *Phys. Rev. C* **64**, 034314 (2001).
 - [26] P. Gögelein, E.N.E. van Dalen, C. Fuchs, and H. Mütter, *Phys. Rev. C* **77**, 025802 (2008).
 - [27] R. Fritz and H. Mütter, *Phys. Rev. C* **49**, 633 (1994).
 - [28] H. Shi, B. Chen, Z. Ma, *Phys. Rev. C* **52**, 144 (1995).
 - [29] E. Schiller and H. Mütter, *Eur. Phys. J. A* **11**, 15 (2001).
 - [30] C. Fuchs, H. Lenske, and H. H. Wolter, *Phys. Rev. C* **52**, 3043 (1995).
 - [31] L. Coraggio, N. Itaco, A. Covello, A. Gargano, and T. T. S. Kuo, *Phys.Rev. C* **68**, 034320 (2003).